招請論文

招請論文 78-15-6-2

영상 System 및 처리의 근황—전산화 3차원 단층 영상처리

(Recent Developments in Imaging Systems and Processings-3 Dimensional Computerized Tomography)

趙 長 熙

(Cho Zang-Hee)

要 約

근래에 발전하고 있는 Artificial Intelligence 또는 Synthetic Image 등 넓은 의미에서의 영상처리에 관하여 해석학적인 설명을 시도하였다.

일반적으로 얻어지는 "영상" 또는 "사진"에 반하여 간접적으로 얻어진 Synthetic Image의 대표적인 예로서 3차원 영상 재 구성(3-Dimensional Image Reconstruction)을 들 수 있으며, 이의 최근 의학 및 생명 과학 분야는 물론 공학 및 물리학 분야의 비파괴 검사(NDT)등 많은 분야에의 응용에 급격한 발전을 보고 있다.

본 논문은 3차원 CT (Computerized Tomography)의 기본을 이루는 3차원 영상 재구성 처리에 관한 기본적인 문제를 two-dimensional signal processing의 관점에서 다루었다.

Abstract

Recently developed Computed Tomography (CT) reconstruction algorithms are reviewed in a more generalized sense and a few reconstruction examples are given for illustration. The construction of an image function from the physically measured projections of some object is discussed with reference to the least squares optimum filters, originally derived to enhance the signal-to-noise ratio in communications theory. The computerized image processing associated with tomography is generalized so as to include 3 distinct parts; the construction of an image from the projection, the restoration of a blurred, noisy image, degraded by a known space-invariant impulse response, and the further enhancement of the image, e.g. by edge sharpening. In conjunction with given versions of the popular convolution algorithm, not to be confused with filtering by a 2-diminsional convolution, we consider the conditions under which a concurrent construction, restoration, and enhancement are possible. Extensive bibliographical lists are given in the references.

1. Introduction

Computerized Tomography (CT), or more specifically, Computerized Transverse Axial Tomography (CTAT), is now widely known within the community of physical scientists and medical practitioners [1,2]. In a sense, practical tomography, whose fruition is generally credited to G.N. Hounsfield of EMI Ltd., Great Britain, is a remarkable achievement. It has developed into a working option for physicians, and evidently, many hospitals desire this type of diagnostic equipment.

The processing which leads to the resultant

*正會員, 韓國科學院電氣 및 電子工學科
(Dept. of Electrical Science, KAIS)
接受日字 : 1978年 9月 14日

image could be realized in various ways. High speed general purpose computers have been used, as have the slower minicomputers; it is clear, in this day and age, that specialized processing or microprocessing, e.g. "hardwired" FFT, convolution, or back-projection, can be realized with great efficiency.

The underlying theoretical reasons as to why this processing hardware is necessary can be explained by a 2-dimensional Fourier analysis, as we shall eventually do; but it should be mentioned that the necessary process can also be discovered by physical reasoning in the spatial domain. A sample slice from a Transverse Axial (TA) mode scan, for example, suggests that beams of uniform intensity, from all angles, should be back-projected and superimposed (see Fig. 1). But the resultan image was found to be badly distorted by an excessively high, slowly varying intensity near origin or center, leading one to search for a suitable method of compensation. By convolving the projected values with a certain "histogram" before they are back-projected, the characteristic distortion can, for all practical purposes, be removed.

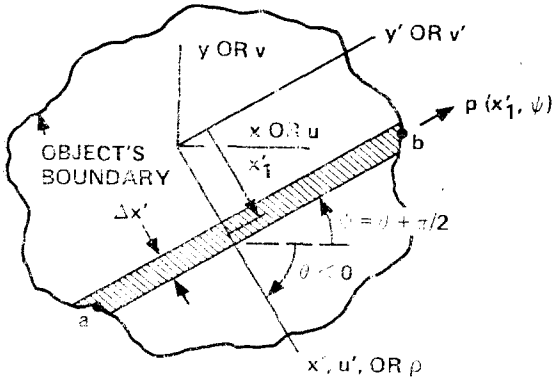

Fig.1. The value of a projection $p(x_1'\psi)$., of an object, is defined to be the line integral between a and b along $y=-x/\tan(\theta)+x_1'/\sin(\theta)$. This line integral can be approximated by direct measurement in the strip of width $\Delta x'$. During a back-projection, this strip is taken to be a beam of uniform intensity. Also shown are the spatial (x,y) and spatial frequency (u,v) or (ρ,θ) variables.

By introducing a frequency domain, the necessary compensation can be defined as a "linear," zero phase, circularly symmertric weighting $|\rho|$. In fact, the necessary function occurs naturally during a cartesian to polar coordinate transformation of the Fourier equations. This transformation is convenient because the projection values are collected in polar geometry.

Filtering of an object function $O(u,v)$, u and v being the spatial frequency, or frequency variables along the x and y spatial directions, implies, in this article, a simple weighting in frequency domain, e.g. by a filter function $H(u,v)$:

$$I(u,v)=H(u,v)O(u,v). \tag{1}$$

The result, $I(u,v)$, a filtered version of $O(u,v)$, ts an approximation to the object function: we call it the image function. The filter function $H(u,v)$ might be considered to be a frequency domain window whose value is zero beyond the window's boundary: or $H(u,v)$ might be an optimal noise or an optimal restoration filter, or ismply a function which somekhow enhances the resultant spatial domain image. The spatial domain image, incidently, is obtained by inverse Fourier transformation:

$$I(x,y)=\int_{-\infty}^{\infty}\int_{-\infty}^{\infty} I(u,v)\exp[2\pi j(ux+vy)]\,du\,dv \tag{2}$$

Latter, we will mention the conditions on $I(u,v)$, $O(u,v)$, and $H(u,v)$ which guarantee that the Fourier analysis can be applied.

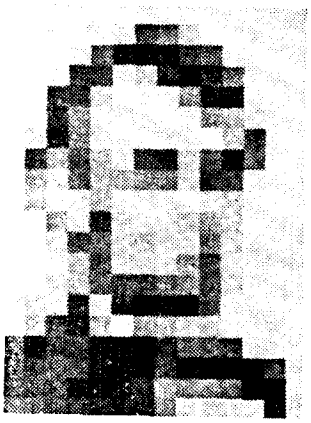

Fig.2. A digital image as it appears when displayed with 15×20 blocks or pixels (courtesy L.D. Harmon and B. Julesz, Sci., V. 180, pp. 1194~1196, 1973).

The imoprtance of 2-dimensional filtering can be demonstrated by way of Fig.2. This is a digitized picture whose total storage requirements are modest, and which could be transmitted efficiently by electrical means [3]. This kind of coarse picture can be mapped into an object space $O(x,y)$, Fourier transformed to $O(u,v)$, filtered by an appropriate $H(u,v)$, and transformed to the image $I(x,y)$ as in Fig.3. Here a simple low pass filter was used; its cutoff frequency was $0.6/\Delta x, \Delta x$ being the block interval of the original coarse picture. Unquestionably, the filtered image is enhanced in the mind of the viewer, the human perception being enhanced by the removal of sharp, high frequency edges.

Fig.3. The image which appears when Fig.2 is processed through a 2-dimensional low pass filter (courtesy L.D. Harmon and B. Julesz).

In opposition to the above instance, there are images whose edges might be accentuated [4]. Enhancement includes smoothing, edge crispening, ripple removal, echo selection, echo rejection and dynamic range control. The filter function $H(u,v)$, together with the $|\rho|$ function, appears naturally and can be realized, except for digital error, in the processing which forms the core of 2 and 3-D image reconstruction.

2. Two-dimensional Filtering and the Fourier-convolution Procedure

We now turn our attention to a version of Fourier analysis in polar coordinates which can be used to construct images from the projections of an object [5]. Let $O(u,v)$ be the Transform of the object function $O(x,y)$, i.e.

$$O(x,y)=\int_{-\infty}^{\infty}\int_{-\infty}^{\infty}O(u,v)e^{2\pi j(ux+vy)}\,dudv. \tag{3}$$

The "$\pm\infty$" notation denotes the usual limit of the integral as the variables of integration are made to increase without bound. The limit will exist if the following exists

$$L_1=\int_{-\infty}^{\infty}\int_{-\infty}^{\infty}|O(u,v)|\,dudv \tag{4}$$

i.e. if L_1 is bounded. In polar coordinates in the frequency domain the following relations apply

$$u=\rho\cos\theta$$
$$v=\rho\sin\theta \tag{5}$$

and

$$du\,dv=\rho\,d\rho d\theta. \tag{6}$$

It may be noted that the ρ of Eq. (6) is equivalent to the Jacobian determinant which relates differential area in u,v, space to differential area in ρ,θ space, i.e.

$$\begin{vmatrix}\frac{\partial u}{\partial\rho} & \frac{\partial u}{\partial\theta}\\ \frac{\partial v}{\partial\rho} & \frac{\partial v}{\partial\theta}\end{vmatrix}=\rho$$

The Fourier transform, Eq. (3), can be expressed in polar coordinates as

$$O(x,y)=\int_0^{2\pi}d\theta\int_0^{\infty}d\rho\;\rho\,O(\rho,\theta)e^{2\pi j\rho x'}. \tag{8}$$

By virtue of the Hermitian symmetry of the integrand, we can write

$$O(x,y)=\int_0^{\pi}d\theta\int_{-\infty}^{\infty}d\rho\;|\rho|\;O(\rho,\theta)e^{2\pi j\rho x'} \tag{9}$$

where $x'=x\cos\theta+y\sin\theta$.

As we showed in Eq. (1), the $O(\rho,\theta)$ could have been processed through a 2-dimensional filter $H(\rho,\theta)$, i.e.

$$I(\rho,\theta)=H(\rho,\theta)O(\rho,\theta), \tag{10}$$

where

$$H(\rho,\theta)\leq B,\ \text{any}\ \rho,\theta, \tag{11}$$

and B denotes a finite bound.

Such processing is permissible because Eq. (3), Eq. (4), and hence Eq. (9) continue to exist when $O(\rho,\theta)$ is replaced by $I(\rho,\theta)$:

$$I(x,y)=\int_0^{\pi}d\theta\int_{-\infty}^{\infty}d\rho|\rho|\;I(\rho,\theta)e^{2\pi j\rho x'} \tag{12}$$

The inner integral of Eq. (12), which we will

define as $f(x,'\theta)$ can be written as

$$f(x',\theta)=\int_{-\infty}^{\infty} d\rho\ [|\rho|\ H(\rho,\theta)]\ O(\rho,\theta)e^{2\pi j\rho x'} \quad (13)$$

Consider the 1st term in brackets in the integrand; we define it as $\Phi(\rho,\theta)$:

$$\Phi(\rho,\theta)=|\rho|\ H(\rho,\theta). \quad (14)$$

This function will be seen to be a central parameter in image construction: the factor $|\rho|$ can be interpreted as the radial frequency compensation term, removing the characteristic distortion of a simple back-projection and superposition of the projected values, as discussed in the introduction. In connection with this discussion, the outter, 0 to π integration of Eq. (12) is analogous to the superposition operation. And then $H(\rho,\theta)$ is the filter function which may optimize the signal relative to the noise, enhance the resultant image, or serve as an inverse filter for the purpose of restoration. In the simplest, unfiltered case, equivalent to a unit transfer of infinite bandwidth, $H(\rho,\theta)=1$ at all frequencies in ρ,θ space.

In order to proceed with the derivation of the Fourier convolution method, the 1-dimensional Fourier transform, termed $\xi(x')$, of $\Phi(\rho,\theta)$ is required to exist:

$$\xi(x')=\int_{-\infty}^{\infty} d\rho\Phi(\rho,\theta)e^{2\pi j\rho x'} \quad (15)$$

Equivalently,

$$L_2=\int_{-\infty}^{\infty} d\rho|\rho|\ |H(\rho,\theta)|\leq B' \text{ for any } \theta, \quad (16)$$

where B' denotes a finite bound. It is evident tnat the condition Eq. (11) is insufficient, and that $H(\rho,\theta)$ must also cause L_2 to be bounded. This tougher condition implies, for instance, that $H(\rho,\theta)$ must approach zero faster than $1/|\rho|^3$ as $|\rho|$ increases without bound. Within the restriction of Eq. (16), $H(\rho,\theta)$ can be any filter function: low, band, or highpass, restoration or enhancement.

Other, more specialized properties can be attributed to, or imposed on $H(\rho,\theta)$; e.g. it must be linear. It must be derived from a space-invariant 2-dimensional impulse response, or a shift-invariant $\xi(x')$. Because $I(x,y)$ must be real, $I(\rho,\theta)$ must have Hermitian symmetry at fixed θ. Hence $H(\rho,\theta)$ must be Hermitian as well. Ordinarily, it is sufficient to allow the imaginary part to be zero, making $H(\rho,\theta)$ "resistive". When $H(\rho,\theta)$ is resistive, $\xi(x')$ can be computed to be a cosine transform, i.e.

$$\xi(x')=2\int_0^{\infty} d\rho\ \rho\ H(\rho,\theta)\ \cos\ (2\pi\rho x') \quad (17)$$

When one desires to treat equally the waves along differing directions, he must merely make $H(\rho,\theta)$ circularly symmetric. When this has been done, we write $H(\rho,\theta)$ as $H(\rho)$.

$H(\rho,\theta)$ is indispensible to the Fourier-convolution procedure because it serves to limit the otherwise unbounded $|\rho|$. This makes possible the numerical computation of $\xi(x')$; but perhaps more importantly, $H(\rho,\theta)$ prevents $|\rho|$ from amplifying the high frequency noise in that domain where the spectral components of the image are insignificant. The optimum shape of $H(\rho,\theta)$ is now considered.

In order to generalize our approach, it will be assumed that the object function is distorted by a given filter function, termed $H_1(\rho,\theta)$, and that 2-dimensional noise is added to the distorted result. The inverse Fourier transform of $H_1(\rho,\theta)$, known as the impulse response, or the point spread function, is space invariant; it provides a convenient way to characterize the distorting influence. In photography, for instance, one can define an impulse response for the distortion caused by a lack of optical focus, by relative motion between the subject and the camera during the exposure, by finite shutter speed, and by the optical effect of atmospheric turbulence [6]. A simple Gaussian spread effectively characterizes various types of circularly symmetric point spread functions, e.g.

$$h_1(r)=\exp\ [-r^2/2\sigma^2]/2\pi\sigma^2 \quad (18)$$

wherer σ^2 is variance, and r is distance from the impulse or point of excitation. Given an image, corrupted by a space-invariant point spread, the distortion can be effectively attenuated by a matched, or inverse filter which negates the effect of $H_1(\rho,\theta)$. As is known, an optimum inverse filter function can be found which (removes noise in such a way that it) minimizes the mean square difference between points of the object

and the estimated image functions [7]. In general, it can be written as

$$H(\rho,\theta)=\frac{H_1^*(\rho,\theta)\ \Psi_0(\rho,\theta)}{|H_1(\rho,\theta)|^2\ \Psi_0(\rho,\theta)+\Psi_n(\rho,\theta)} \tag{19}$$

where $\Psi_0(\rho,\theta)$ and $\Psi_n(\rho,\theta)$ are the power spectral densities of the object and the noise signals, respectively. These may be estimated by analyzing portions of a reconstructed object, the noisy version, as it appears when passed through a low pass filter with a relatively high cutoff frequency [7]. Latter, we will discuss a method of computing power spectra estimates. In order to obtain an estimate of the optimum image of the first slice of some object, at least 2 constructions are necessary: one for the broad band, unoptimized image, and one for the estimate of the optimum image. However, it may be reasonable to employ the same power spectra functions for additional slices of the same object, because the final image is not a strong function of the details of the power spectra.

If one assumes a Gaussian spread, as in Eq. (18) and also that $\Psi_n(\rho,\theta)/\Psi_0(\rho,\theta)$, termed $n(\rho,\theta)$, exists at all frequencies, the optimum function can be written as

$$H(\rho,\theta)=\frac{\exp[-2\pi^2\sigma^2\rho^2]}{\exp[-4\pi^2\sigma^2\rho^2]+n(\rho,\theta)} \tag{20}$$

In a blurred picture, for instance, one may suspect a defocused camera but he may not know the variance of the point spread function which characterizes the defocusing. In such a case it is reasonable to try a few values of σ and to choose the one which results in the clearest, most pleasing final image.

In the noiseless case, Eq. (20) simplifies to

$$H(\rho)=\exp[+2\pi^2\sigma^2\rho^2], \tag{21}$$

which obviously must be set to zero beyond a certain radial frequency. A truncation occurs naturally when $n(\rho,\theta)$ is included; infact, at fixed θ, the cutoff becomes quite sharp once $\exp[-4\pi^2\sigma^2\rho^2]<n(\rho,\theta)$ as suggested by Fig.4. This is because $\Psi_0(\rho,\theta)$ generally drops much faster than $\Psi_n(\rho,\theta)$ especially if the noise power spectrum is white, or constant. A typical power spectrum of an image is given in Fig.5. Fig.6 is the reconst-

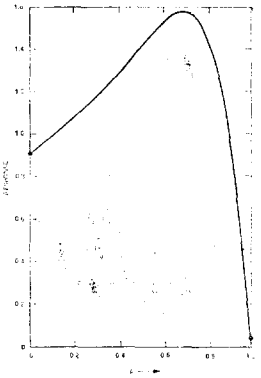

Fig.4. The general form of an inverse filter which compensates for a Gaussian point spread or impulse response.

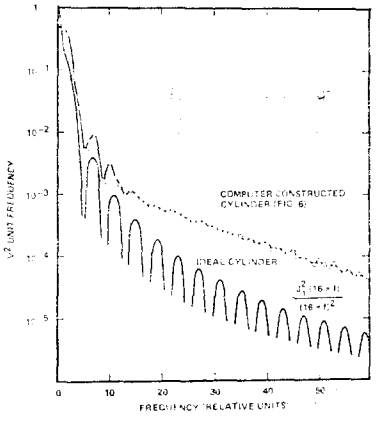

Fig.5. The power spectra of circularly symmetric images. The frequency has been multiplied by 64 so that 1 cycle per unit distance is equal to 64 frequency units.

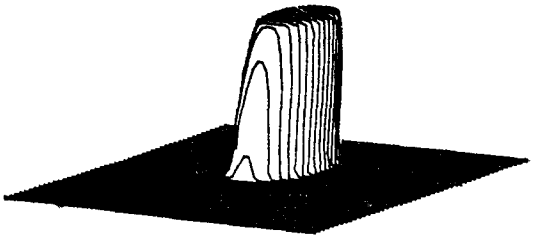

Fig.6. An image of a cylinder. This image was constructed by LSC, i.e. by the compensation, back projection, and the linearsuperposition of the projection data of an ideal cylinder (based on 180 views and an 80×80 array).

ructed image whose spectrum was estimated as shown in Fig.5. As shown, the spectral power decreases rapidly as frequency increases, especially in the low frequency domain.

When $H_1(\rho,\theta)=1$, a particularly simple and well known noise filter follows from Eq. (19)

$$H(\rho,\theta)=\frac{\Psi_0(\rho,\theta)}{\Psi_0(\rho,\theta)+\Psi_n(\rho,\theta)} \tag{22}$$

Here $H(\rho,\theta)$ may approach a sharp cutoff, or ideal low pass filter. If there is reason to believe that the power spectra are circularly symmetric, as they should be in the case of a cylinder and white noise, then Eq. (22) approaches a simple, circularly symmetric, low pass filter function.

At this point the details of the Fourier-convolution procedure will be resumed and completed.

By fixing θ at θ_1, a 1-dimensional transform of $O(\rho,\theta_1)$ can be found. It now becomes necessary to define the term $p(x',\phi)$ as the line integral through the object function $O(x,y)$:

$$p(x',\phi)=\int_a^b dy' O(x',y'). \tag{23}$$

$O(x',y')$, the object function expressed in a rotated coordinate system, is assumed to be zero outside of its boundary; $p(x',\phi)$ can be closely approximated by physical measurement in a strip of finite width $\Delta x'$ (see Fig.1).

We will now introduce a relation which has come to be called the "projection-slice theorem" [8]. In short, this theorem states that

$$p(x',\phi_1)=F_1^{-1}\{O(p,\theta_1)\}, \tag{24}$$

where F^{-1} denotes the inverse 1-dimensional Fourier transform operation, and θ_1 and ϕ_1 are fixed values of θ and ϕ. The proof of Eq. (24) is as follows: The 1-dimensional transform of Eq. (23) is

$$F_1\{p(x',\phi_1)\}=\int_{-\infty}^{\infty} dx' e^{-2\pi j u' x'}\int_a^b dy'\, O(x',y') \tag{25}$$

$$=\left[\int_{-\infty}^{\infty} dx' \int_{-\infty}^{\infty} dy'\, O(x',y') e^{-2\pi j(u'x'+v'y')}\right]_{v'=0} \tag{26}$$

Therefore Eq. (25) is the 2-dimensional transform of $O(x',y')$ on the line $v'=0$ or $\theta=\theta_1$, i.e. it is $O(\rho,\theta_1)$.

Returning to our explanation of the 1-dimensional convolution method, we have established the following transform pairs:

$$\xi(x')=F_1^{-1}\{\Phi(\rho,\theta)\} \tag{27}$$

$$p(x',\phi_1)=F_1^{-1}\{O(\rho,\theta_1)\}. \tag{28}$$

Therefore, by the convolution theorem, Eq. (13) can be expressed as

$$f(x',\theta)=\xi(x')*p(x',\phi). \tag{29}$$

The image function which follows from Eq. (12) is

$$I(x,y)=\int_0^{\pi} d\theta\, f(x',\theta) \tag{30}$$

where $x'=x\cos(\theta)+y\sin(\theta)$ and $\theta=\phi-\pi/2$.

Equations (29) and (30) express, in continuous form, the Fourier-convolution procedure. It is characterized by strictly real operations in polar coordinates. We will now consider the digita implementation of (29) and (30).

3. The Digital Implementation of the Fourier-convolution Procedure.

We will first imagine that $I(x,y)$ is represented in sampled form on a grid. In approximating Eq (30), the values of $f(x',\phi)$ must be summed, or superimposed at the sample points, i.e.

$$I(x_m,y_n)=\sum_{j=1}^{NV} f(x',\phi_j),\quad 1\le m,n\le N, \tag{31}$$

where NV=the number of descrete views(ϕ_j). At a given view, the 1-dimensional $f(x',\phi_j)$ can be imagined as being "back-projected" across the entire plane. The problem, here, is that $f(x',\phi_j)$ will be available only at descrete x_i', necessitating an interpolation to the sample points, a linear interpolation being most logical [9].

An important aspect of digitization is the selection of values for $\xi(n\Delta x')$, where $\Delta x'$ is the scanning beam width, and $n=0,1,2,3,N-1$. The $\xi(n\Delta x')$ values are to be convolved with the $p(n\Delta x',\phi)$ values, as suggested by Eq. (29). We first consider numerical quadrature of Eq. (17), the cosine transform. Our procedure involves approximating the average of $\xi(x')$ within $\Delta x'$, and assigning the average values to the respective $\xi(n\Delta x')$. In order to provide a simple illustration, $H(\rho,\theta)$ will be assumed to be a circularly symmetric low pass filter function. The result of a particular set of calculations is given in Fig.7.

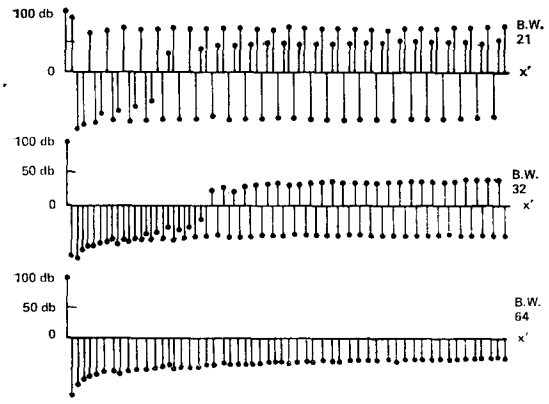

Fig.7. These spatial domain $\xi(n\Delta x')$ were computed from low pass filter functions; three different cutoff frequencies, or bandwidths (B.W.), were used. The bandwidth units are scaled so that 1 cycle/unit distance equals 64 frequency units. Positive values of $\xi(n\Delta x')$ were mapped into the positive portion of the y-axis according to $20\log_{10}[\xi(n\Delta x')]$; negative values of $\xi(n\Delta x')$ were mapped into the negative portion of the y-axis according to $-20\log_{10}|\xi(n\Delta x')|$; and $n=0,1,2,3,4,7,9$.

Special cases of the above procedure may be found in [5,9,10].

The filter function $H(\rho,\theta)$ cannot be realized exactly because of digital error. Assuming, for the moment, that the number of views NV can be made sufficiently large so as to make the angular digitization error insignificant, $\xi(n\Delta x')$ can be viewed as a 1-dimensional digital filter, approximating a given radial line of the 2-dimensional filter function $H(\rho,\theta)$. Sampling techniques can be used in the design of such a filter only if the input signal, $O(x,y)$ is bandlimited' i.e., if

$$O(\rho,\theta)=0,\quad \rho>\text{B.W. (bandwidth)}. \tag{32}$$

When the above conditions are satisfied, the design techniques of "windowing" or "frequency sampling" can cause the realized filter to be as close as possible, at a fixed N, to the $H(\rho,\theta)$ function [11, pp.239~268].

A spatial-domain approach by Cho, et al, has realized a certain $H(\rho)$ with a very high bandwidth [12, 13]. In this approach $\Phi(\rho)$, assumed to be circularly symmetric, is equated to $|\rho|$. It is recognized that without $|\rho|$, the impulse response in the 2-dimensional spatial domain is distorted into a $1/r$ spread.

The $\xi(n\Delta x')$ are computed by forcing successive values to approximately compensate for the $1/r$ function. Typically used $\xi(n\Delta x')$, sometimes called "correction" or "deblurring" functions, are graphed in Fig.9. These seem to fall off faster than those of Fig.7: this is partly because the Fig. 7 functions are derived from lower bandwidth filter functions. If desired, the Fig. 7 functions could be tailored with a window, e.g. a Blackman window, as in Fig.9. Windows were found to not harm the desired filtering action.

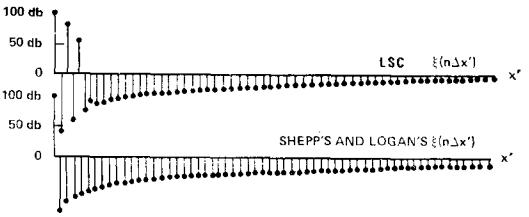

Fig.8. These are examples of those $\xi(n\Delta x')$ which are most used in image reconstruction. The scales are the same as the scales of Fig.7.

Digital Techniques which Construct Images Composed of Pixels. Programs based on sampling, an interpretation sometimes given to Shepp's and Logan's program, are not entirely compatible with inputs which are averages over $\Delta x'$. However, the program based on linear interpolation creates an entirely satisfactory image (L.A. Shepp and J.B. Kruskal, "Computerized tomography: the new medical X-ray technology," published in the American Mathematical Monthly). The desire for compatibility with input beams, output pixels, and the elimination of interpolation in images has lead to some interesting approaches Fig.10 shows that by calculating the beam-pixel overlap, or weighting factors, one can generate equations based on area averaged, actually

$$f(r,\phi) = \int_0^{\pi} \left[p(x',\theta) * \mathcal{F}^{-1}[\rho] \right] d\theta$$

$\mathcal{F}^{-1}[\rho]$ convolution kernel

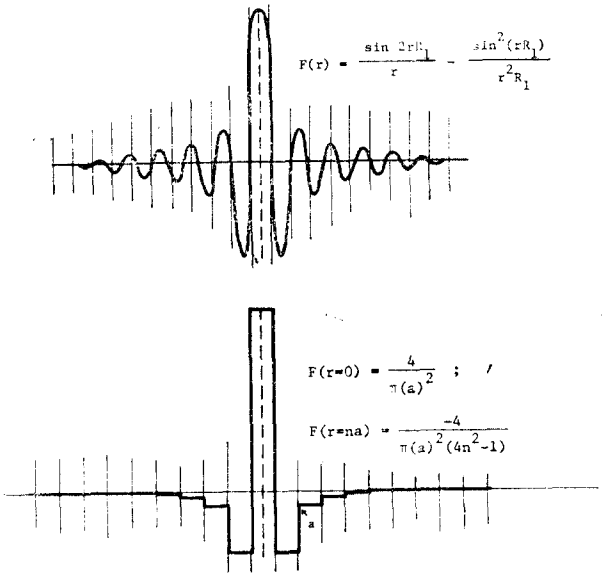

Fig.9. These are same as the LSC and Shepp's filter functions shown in Fig. 8 in linear scale.

volume averaged physical properties of the media. Programs have been devised to compute the weighting factors at each angle, beam, and pixel, typical dimensions being 180° 1° steps, 80 or 160 beams, and 80×80 or 160×160 pixels [13]. The weighting factors are usually placed on a disk-file and called into core as they are needed. At each beam of a given angle, the storage is arranged so that about 150 real factors are mapped to their respective pixels by about 150 concomitantly stored pointers.

The LSC, or Linear Superposition with Compensation, is essentially equivalent to the above discussed Fourier convolution procedure, except that precalculated weighting factors are used to perform the superposition, as in Fig.10: the compensation is provided by Cho's $\xi(n\Delta x')$, the one derived in the spatial domain. After convolution with $\xi(n\Delta x')$, the projected values are backprojected and superimposed. The weighting factors create a high quality, symmetrical image, and because they are precalculated, LSC is almost twice as fast as a program based on linear interpolation between back-projected values. The disadvantages of LSC are that a large data set of precalculated weighting factors is required, at each angle of the construction the program must call for a portion of this external data, and finally, LSC does not permit easy changes in the number of beams per view, the number of views, or the size of the image array.

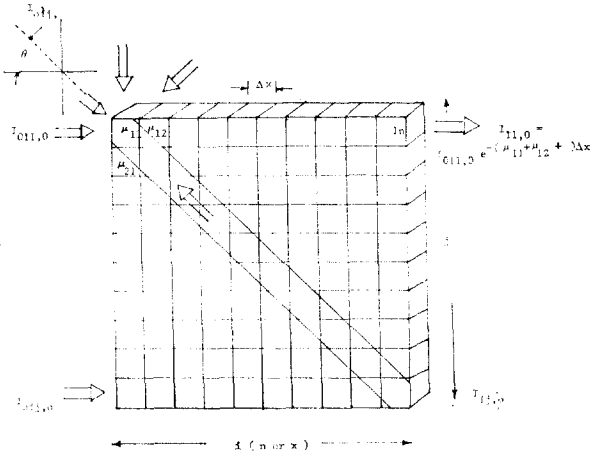

Fig.10. The area (or volume) of a pixel which is overlapped by a beam is termed the "weighting factor", w_{ij}.

One of the iterative algorithms, the least squares iteration, although relatively inefficient and time consuming, deserves mention [14, 15]. A set of scans, as in Fig.10, yields k equations:

$$I = Wu \tag{33}$$

where the dimension of u is $N^2 \times 1$, I is $k \times 1$, and W is $k \times N^2$. Typical dimensions are $k = 180 \times 80 = 14,400$ and $N^2 = 80 \times 80 = 6400$. The least squares iteration of Eq. (33) converges to the unique solution which minimizes the squared difference between the measured projections and the calculated projections of the image. Consequently, this method is noise resistant.

When an optimal noise filter is used, a Fourier-convolution procedure is also noise resistant. Unlike the least squares iteration, this procedure minimizes the squared difference between the true object and the estimated image.

4. The Execution Speeds of Image Construction Algorithms.

If the least squares solution were done exactly, it would be necessary to solve N^2 linear equations; a typical procedure for this purpose, the Gaussian elimination, requires at least $N^6/3$ multiplications. And then, the matrix of coefficients, although very sparse, would be of dimension N^4, which is excessively large. Assuming that weighting factors are used, the least squares iteration approximates the N^2 unknowns in roughly $2kMN^3$ multiplications, M being the number of views, and k the number of iterations, typically 20. The storage is about $2(N^2+MN)$ numbers. Never-the-less this algorithm is one of the least efficient and is not widely used at present.

A reasonable measure of computational complexity, and often, of execution speed, is the total number of real operations, additions, subtractions, localizations, and comparisons necessary to complete a given program.

A 2-dimensional DFT procedure, involving interpolation in the complex frequency domain from a polar to a cartesian grid [8], can be done in about $(3MN+6N^2)\log_2 N+15N^2$ operations, if a FFT algorithm is used. Execution is relatively fast, but complex arithmetic must be used; more significantly, since accurate interpolation, as required, is difficult in the structured, complex frequency domain, a DFT procedure does not always give the sharp image which can be obtained by other methods. Consequently, this procedure is not widely used.

Fourier-convolution algorithms are more popular. Storage requirements are modest, about N^2 numbers. It's easy to discover that Shepp's and Logan's program takes about $16MN^2$ operations, assuming N beams per projection. Our LSC programs take about $11MN^2$ operations. Actually, our Data General minicomputer, a Nova 1200 with disk pack, takes, on a certain construction, 20 minutes with Shepp's and Logan's program, and 14 minutes with LSC. In this case, the time to make 180 calls to a data set of weighting factors is not significant.

5. The Effect of $\xi(n\Delta x')$ and of Noise on the Reconstructed Image.

The Fig.6 cylinder defines a step response whose features, e.g. steepness, depend on the nature, e.g. the bandwidth, of the implied 2-dimensional filter function $H(\rho,\theta)$. This function is approximately realized by way of the $\xi(n\Delta x')$. Various $\xi(n\Delta x')$, derived from a low pass filter, affect the step response of a central half section of a cylinder as in Fig.11. Here it is seen that the LSC function gives the steepest rise because of its greater bandwidth.

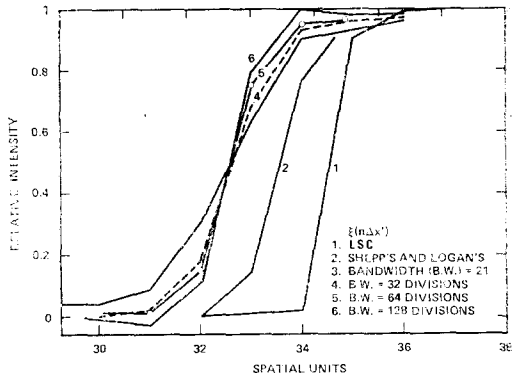

Fig.11. These step transition waveforms are central half sections from images of cylinders, like the one shown in Fig.6. The various images were constructed with the aid of several different types of $\xi(n\Delta x')$.

Image formation by convolution, back-projection and superposition, as described above, depends on a 2-dimensional balance of additions and subtractions, a balance which is upset by noise in the $p(x_i',\phi_j)$, causing widespread error in the final image. For example, if white, or random noise, whose distribution is roughly Gaussian, and whose variance is proportional to the square root of the magnitude of $p(x_i',\phi_j)$, is added to the $p(x_i',\phi_j)$, the Fig.6 cylinder appears as in Fig. 12. The effect appears everywhere and does not particularly depend on the shape of the object.

Fig.12. The reconstructed (LSC) image of the cylinder shown in Fig.6. Severe noise, about 200% maximum added to the line integrals, has ruined the impression of a cylinder.

As has been discussed in connection with equations (19) and (22), the definition of an optimum noise filter depends on a knowledge of the power spectra of the object function and the noise. Consequently, we must consider the estimation of power spectra. Such estimates tend to be crude, especially when the noise sample is small, but they do provide insight into the problem of optimum image processing.

A large diameter noisy disk was constructed as in Fig.13 The power spectrum of the central

Fig.13. The reconstructed (LSC) image of a large, uniform disk. The added noise, in this case, is about 70% maximum.

64×64 points was estimated as described in the appendix. Various $\xi(n\Delta x')$ were used in this construction, and their effect appears in Fig.14. The fluctuations and the differences in the overall shape of these curves are belived to be due to error in the estimate. It seems safe to conclude, however, that above a certain frequency the power decreases, leading one to conjecture that the noise function, like the object function, is filtered by $H(\rho,\theta)$ and $\xi(n\Delta x')$. As we expected, the $\xi(n\Delta x')$ derived by Cho et al passed the higher frequency components, in agreement with the observation that it also produced the sharpest step response.

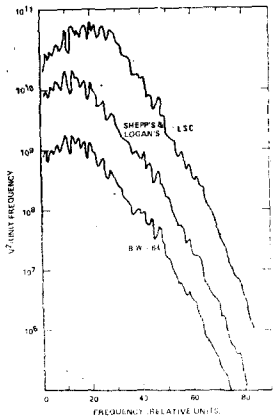

Fig.14. These are estimates of the power spectrum of the 2-dimensional noise in the central portion of images similar to Fig.13. These images were generated by way of 3 different $\xi(n\Delta x')$.

The Fig. 12 image, since it was constructed with a broad band filter, has sharp edges but is excessively noisy. By recomputing this image, using the $\xi(n\Delta x')$ derived from the $H(\rho)$ whose bandwidth is 16 units, one can restore the image of the cylinder. The result appears in Fig.15. The degradation in resolution is also apparent. A truely optimum noise filter would retain as much resolution as possible while reducing the noise to a minimum[9, 16].

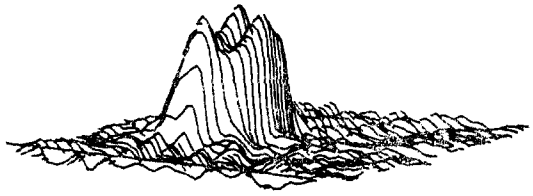

Fig.15. A noisy image, reconstructed by a method similar to the one used in Fig.12. The difference is, the $\xi(n\Delta x')$ was derived from a low pass $H(\rho)$ whose band width is 16 units. The vertical scale is uncalibrated.

Conclusion

We have outlined a generalized approach to reconstruction from projections. When the

measurements contain noise, our approach was to specify $H(\rho,\theta)$ as an optimum, least squares filter function. This optimum function, whose definition depends on an estimate of the power spectra of the noise and of the object, must be derived from a "broadband" version of the, e.g. an image constructed by LSC. So unless the optimum function is known a priori, at least 2 constructions are necessary: the first serves to define the optimum filter function; the second serves to construct the ideally filtered image.

The subject of restoration was touched upon. If it is known that the measured projections are representing an object with a known distortion, i.e. an object signal which has passed through a known filter, then the true object can be approximated by passing the distorted signal through a matched, or inverse filter. Our approach, again, was to specify $H(\rho,\theta)$, or $\Phi(\rho,\theta)=|\rho|H(\rho,\theta)$, as an optimum, least square inverse filter, implying at least 2 image constructions.

Usually, image processing would start with an imperfect image, digitize it in cartesian coordinates, filter it with the appropriately designed filter [17], and then, reconstruct the improved picture. So in a sense, conventional processing always requires 2 image constructions. In tomography the initial image ordinarily is constructed by a Fourier-convolution, or by a LSC procedure. We are suggesting that it is often convenient, during the 1st construction, to realize the desired filtering by way of a judicious formulation of $\Phi(\rho,\theta)$. If this is done, there is no need to construct a blurred image, to filter it, and then to reconstruct the final picture; construction, restoration, and enhancement can be achieved concurrenly.

Acknowledgement: the author is grateful for the comments of Dr. Shepp of Bell Lab., Murrhy Hill, NJ.

REFERENCES

1. Special issue on physical and computational aspects of 3-dimensional image reconstruction, (ed. Z.H. Cho) IEEE Trans. Nuc. Sci., NS-21, 1974.
2. Special issue on advances in picture reconstruction-theory and applications (ed. Z.H. Cho) Comput. Biol. Med., vol. 6, 1976.
3. L.D. Harmon and B. Julesz, "Masking in visual recognition: effects of two-dimensional filtered noise," Sci., V. 180, 1194~1196, 1973.
4. A.V. Oppenheim, R.W. Schafer, and T.G. Stockham, "Nonlinear filtering of multiplied and convolved signals," Proc. IEEE, V. 56, pp.1264~1291, 1968.
5. R.N. Bracewell and A.C. Riddle, "Inversion of fanbeam scans in radio astronomy," Astrophy. J., V. 150, pp.427~434, 1967.
6. T.S. Huang, W.F. Schreiber, and O.J. Tretiak, "Image processing," Proc. IEEE, V.59, pp.1586~1609, 1971.
7. C.W. Helstrom, "Image Restoration by the method of least squares," J. Opt. Soc. America, V. 57, pp.297~303, 1967.
8. R.M. Mersereau and A.V. Oppenheim, "Digital reconstruction of multidimensional signals from their projections," Proc. IEEE, V. 62, pp.1319~1338, 1974.
9. L.A. Shepp and B.F. Logan, "The Fourier reconstruction of a head section," IEEE Trans. Nuc. Sci., NS-21, pp.21~42, 1974.
10. G.N. Ramachandran and A.V. Lakshiminarayanan, "Three dimensional reconstruction from radiographs and electron micrographs; application of convolutions instead of Fourier transforms," Proc. Nat. Acad. Sci. U.S., V. 68, pp. 2236~2240, 1971.
11. A.V. Oppenheim and R.W. Schafer, Digital signal processing. Englewood Cliffs, NJ.: Prentice-Hall, 1975.
12. Z.H. Cho, I. Ahn, C. Bohm, and G. Huth, "Computerized image reconstruction methods with multiple photon/X-ray transmission scanning," Phys. Med. Biol., V.19, pp.511~522, 1974.
13. P. Edholm, "Image reconstruction in trans-

versal computer tomography," Acta Radiol. Supp., V.346, pp. 21~38, 1975.
14. M. Goitein, "Three-dimensional density reconstruction from a series of two-dimensional projections," Nuc. Instr. Meth.,V.101, pp.509~518, 1972.
15. G.T. Herman and A. Lent, "Quadratic optimization for image reconstruction.I" Comput. Graphics and Image Process., V.5, pp. 319~332, 1976. **Appendix 1**
16. E. Tanaka and A. Iinuma, Correction functions and statistical noises in transverse section picture reconstruction, Comput. Biol. Med., V. 6, pp. 295~306, 1976.
17. L.R. Rabiner and B. Gold, Theory and application of digital signal processing. Englewood Cliffs, NJ.: Prentice-Hall, 1975, pp.445~483.

In this appendix an attempt is made to catego rize the references which record the contributions to the theory of 3 D image processing, or which explain the currently used algorithms.

Fourier Methods

1. R.A. Crowther, D.J. DeRosier, and A. Klug, The reconstruction of a three dimensional structure from projections and its application to electron microscopy, Proc. R. Soc. Lond., V.317, pg.319, 1970.
2. D.J. DeRosier and P.B. Moore, Reconstruction of three-dimensional images from electron micrographs of structures with helical symmetry, J. of Mol. Biol., V. 52, pg.355, 1970.
3. D.J. DeRosier and A.Klug, Reconstruction of three dimensional structures from electron micrographs, Nature, V. 217, pg. 130, 1968.
4. O.J. Tretiak, D. Ozonoff, J. Klopping, and M. Eden, Calculation of internal structure from multiple radiograms, Proc. 2D Sig. Processing Conf., U. of Missouri, Columbia, pg. 621, 1971.
5. R.H.T. Bates and T.M. Peters, N.Z.J. of Sci., V. 14, pg.883, 1971.
6. P.R. Smith, T.M. Peters, and R.H.T. Bates, Image reconstruction from finite numbers of projections, J. Phys. A. Math., Nuc. Gen., V. 6, pg. 361, 1973.
7. R.M. Mersereau and A.V. Oppenheim, Digital reconstruction of multidimensional signals from their projections, Proc. IEEE, V. 62, pg. 1319, 1974.
8. D.B. Kay, J.W. Keyes, and W. Simon, J. Nuc. Med., V. 15, pg. 981, 1974.

Fourier-convolution Methods

1. R.N. Bracewell and A.C. Riddle, Inversion of fanbeam scans in radio astronomy, Astropys. J., V. 150, pg. 427, 1967.
2. G.N. Ramachandran and A.V. Lakshiminarayanan, Three dimensional reconstruction from radiographs and electron micrograpahs; application of convolutions instead of Fourier transforms, Proc. Nat. Acad. of Sci., V.68, pg.2236, 1971.
3. D.E.B. Lees, J.W. Keyes, and W. Simon, Reconstruction of radionuclides tomograms by the convolution method, Proc. SPIE Conf. on Applic. of Opt. Inst. in Med. II, Palos Verdes, Calif., 1973.
4. L.A. Shepp and B.F. Logan, The Fourier reconstruction of a head section, IEEE Trans. Nuc. Sci., NS-21, pg.21, 1974.
5. D.A. Chesler and S.J. Riederer, Ripple suppression during reconstruction in transverse tomography, Phys. Med. Biol., V. 20, pg. 632, 1975.
6. H.H. Barrett, S.K. Gordon, and R.S. Hershel, Statistical limitations in transaxial tomography, Comput. in Biol. and Med., V. 6, pg. 307, 1976.
7. E.Tanaka, Statistical noise of reconstructed image in transverse scan, IV-th Int. Conf. on Inform. Process. in Scintigraphy, Orsay, 1975.

Fourier Transforms in General

1. R.N. Bracewell, The Fourier transform and its applications. N.Y.: McGraw Hill, 1965.

2. J.W. Goodman, Introduction to Fourier Optics. N.Y. McGraw Hill, 1968.
3. E.O. Brigham, The fast Fourier transform. N.J.: Prentice Hall, 1974.

Spatial Methods: Linear Superposition with Compensation (LSC) or Filtered Back-projection

1. C.A.G. LeMay, US Pat. No. 3924199, Method and apparatus for constructing a representation of a planar slice of a body exposed to penetrating radiation, Dec. 2, 1975.
2. Z.H. Cho, I. Ahn, C. Bohm, and G.C.Huth, Computerized image reconstruction methods with multiple photon/X-ray transmission scanning, Phys. Med. Biol., V.19, pg. 511, 1974.
3. Z.H. Cho and I. Ahn, Computer algorithm for the tomographic image reconstruction with X-ray transmission scan, Comput. and Biol. Research, V. 8, pg.8, 1975.
4. P. Edholm, Image reconstruction in transversal computer tomography, Acta Radiol. Suppl., V. 346, pg.21, 1975.
5. E. Tanaka and T.A. Iinuma, Correction functions for optimizing the reconstructed image in transverse section scan, Phys. Med. Biol., V.20, pg. 789, 1975.
6. E. Tanaka and A. Iinuma, Correction functions and statistical noises in transverse section picture reconstruction, Comput. Biol. Med., V.6, pg. 259, 1976.
7. B.K. Vainshtein and S.S. Orlov, General theory of direct 3-D reconstruction, Symposium Proceedings of an International workshop on Techniques of Three Dimensional Reconstruction, Brookhaven National Laboratory, Upton, New York, July 16~19, 1974.

Iterative Reconstruction Methods

1. G.N. Hounsfield, UK Pat. No. 1283915, A method of and apparatus for examination of a body by radiation such as X-ray or gamma radiation, London, 1972.
2. R. Gordon, R. Bender, and G.T.Herman, Algebraic reconstruction technique (ART) for three dimensional electron microscopy and X-ray photography, J. of Theor. Biol., V.29, pg. 471,1970.
3. G.T. Herman, A Lent, and S.W. Rowland, ART: mathematics and applications, J. Theor. Biol., V.42, pg. 1, 1973.
4. M. Goitein, Three dimensional density reconstruction from a series of two-dimensional projections, Nuc. Instr. and Meth., V.101, pg.509, 1972.
5. P. Gilbert, Iterative methods for the three dimensional reconstruction of an object from projections, J. of Theor. Biol., V.36, pg. 105, 1972.
6. R. Gordon, A tutorial on ART, IEEE Trans. Nuc. Sci., NS-21, pg. 78,1974.
7. G.T. Herman, A relaxation method for reconstructing objects from noisy X-rays, Math. Prog., V.8, pg.1, 1975.
8. B.E. Oppenheim, More accurate algorithms for iterative 3-D reconstruction, IEEE Trans. Nuc. Sci., NS-21, pg. 72, 1974.
9. G.T. Herman and A. Lent, Iterative reconstruction algorithms, Comput. Biol. Med., V.6, pg. 273, 1976.
10. T.F. Budinger and G. Gullberg, Three dimensional reconstruction in nuclear medicne, IEEE Trans. Nuc. Sci., NS-21, pg.1, 1974.

Other Methods

1. J. Radon, On the determination of functions from their integrals along certain manifolds, Berichte Saechsische Akad. Wissenschaft., Leipzig, V.69, pg.262, 1917.
2. J. Beattie, Tomographic reconstruction from fan beam geometry using Radon's integration method, IEEE Trans. Nuc. Sci., NS-22, pg. 359, 1975.
3. A.M. Cormack, Representation of a function by its line integrals, with some radiological applications, J.Appl. Phys., V.34, pg.2722, 1963.

4. A.M. Cormack, Reconstruction of densities from their projections, with applications to radiological physics. Phys. Med. Biol., V. 18, pg. 195, 1973.
5. R.B. Marr, On the reconstruction of a function on a circular domain from a sampling of its line integrals, J. of Math. Anal. and Appl., pg. 357, 1974.
6. J.S. Robertson, R.B. Marr, M. Rosenblum, V. Radeka, and Y.L. Yamamoto, 32-crystal positron transverse section scanner, Tomographic Imaging in Nuc. Med. (Society of Nuc. Med., NY.) pg. 142, 1973.

Fan Beam Reconstruction Methods

1. A.V. Lakshiminarayanan, Reconstruction from divergent ray data, Tech. Rpt. 92, Dept. of Comput. Sci., State U. of NY., Buffalo, 1975.
2. G.T. Hermann, A.V. Lakshiminarayanan, and A. Naparstek, Reconstruction using divergent ray shadowgraphs, Workshop on Recon. Tomog. in Diag. Radiol. and Nuc. Med., Puerto Rico, 1975, In press.
3. Z.H. Cho, L. Eriksson, and J. Chan, A circular ring transverse axial positron camera, Workshop on Recon. Tomog. in Diag. Radiol. and Nuc. Med., Puerto Rico, 1975.
4. Z.H. Cho, C.M. Tsai, I. Ahn, L. Wang, and J.R. Parsons, Pseudo fan beam reconstruction algorithms and their related physical problems, IEEE Trans. Nuc. Sci., NS-23, pg. 560, 1976.
5. J.P. Stonestrom and A. Macovski, Scatter considerations in fan beam computerized tomographic systems, IEEE Trans. Nuc. Sci., NS-23, pg. 1453, 1976.
6. D. Boyd, J. Dehnert, et al, High pressure xenon proportional chamber for X-ray laminographic reconstruction using fan beam geometry, IEEE Trans. Nuc. Sci., NS-21, pg. 184, 1974.
7. G.T. Hermann, A.V. Lakshiminarayanan, and A. Naparstek, Convolution reconstruction techniques for divergent beams, Comput. Biol. Med., V.6, pg. 259, 1976.

Review Papers

1. T.F. Budinger and G.T. Gullberg, Three-dimensional reconstruction in nuclear medicine emission imaging, IEEE Trans. Nuc. Sci., NS-21, pg.1, 1974
2. Z.H. Cho, General views on 3-D image reconstruction and computerized transverse axial tomography, IEEE Trans. Nuc. Sci., NS-21, pg. 44, 1974.
3. G.T. Herman and R. Gordon, Three-dimensional reconstruction from projections, a review of algorithms Int. Rev. Cytol., V. 38, pg.111, 1974.
4. G.T. Herman and S.W. Rowland, Three methods for reconstructing objects from X-rays: a comparative study, Comput. Graphics and Image Process., V.2, pg. 151, 1973.
5. Z.H. Cho, J. Chan, E. Hall, R. Kruger, and D. McCaughey, A comparative study of 3-D image reconstruction algorithms with reference to number of projections and noise filtering, IEEE Trans. Nuc. Sci., NS-22, pg. 344, 1975.
6. R. Brooks and G. DiChiro, Theory of image reconstruction in computed tomography, Radiol., V. 117, pg. 561, 1975.
7. L.A. Shepp and J.B. Kruskal, Computerized tomography: the new medical X-ray technology, published in American Math. Monthly, Vol.85, No.6, July 1978.

Appendix 2

A note on the estimation of 2-dimensional power spectra A 1-dimensional power spectrum [11, pp. 532~548] is the Fourier transform of the autocovariance function, which, in a zero mean process, is identical to the autocorrelation function. The autocorrelation of a N-point sequence can be estimated as

$$c_{xx}(m)=\frac{1}{N}\sum_{n=0}^{N-|m|-1} x(n)\times(n+m),\quad |m|<N$$

(A-1)

If one were to multiply by $N/(N-|m|)$, the average of $x(n)\times(n+m)$ would result; and if one could take the limit of the average of $x(n)\times(n+m)$ as $N\to\infty$, he would obtain the definition of the descrete autocorrelation.

The sequence $x(n)\times(n+m)$ of Eq. (A-1) is effectively weighted by

$$w_B(m)=\begin{cases}\dfrac{N-|m|}{N}, & |m|<N\\ 0 & \text{otherwise;}\end{cases} \qquad \text{(A-2)}$$

A heuristic explanation of the utility of this triangular or Bartlett "lag" window can be given in continuous m-space, assuming the existance of the autocorrelation $c(m)$ and the power spectrum $P(f)$: if

$$c_{xx}(m)=w_B(m)c(m) \qquad \text{(A-3)}$$

then

$$P_{xx}(f)=W_B(f)*P(f) \qquad \text{(A-4)}$$

$W_B(f)$ has a main peak and many side maxima, and causes the estimate $P_{xx}(f)$ to approach $P(f)$.

The Bartlett window has some significant computational advantages. For instance, the Fourier transform of $c_{xx}(m)$ is

$$I_N(f)=\sum_{m=-(N-1)}^{N-1} c_{xx}(m)\ \exp\ (-2\pi\ jfm), \qquad \text{(A-5)}$$

but it can be shown that

$$I_N(f)=\frac{1}{N}|X(f)|^2 \qquad \text{(A-6)}$$

where $X(f)$ is the ordinary DFT of the sequence $x(n)$, $0\le n\le N-1$:

$$)=\sum_{n=0}^{N-1} x(n)\ \exp(-2\pi jfn) \qquad \text{(A-7)}$$

$I_N(f)$ is called the "periodogram" and approximates the power spectrum of $x(n)$.

Unfortunately the variance of $I_N(f)$ does not vanisheas $N\to\infty$ (see Oppenheim and Schafer, op. cit., p. 542). A standard approach which reduces the variance is to average over a number of independent estimates of $I_N(f)$, e.g. by dividing the sequence into K segments and computing K periodograms. For our purposes the standard technique is modified as follows: The 2-dimensional periodogram of $N\times N$ samples is computed by a 2-dimensional DFT; if circular symmetry can be assumed, the frequency domain values of $I_{N\times N}(u,v)$ near circles(concentric about the orgin) are averaged. This procedure is justified when the object is circularly symmetric, or when the samples are of random noise, because in these cases one expects a circularly symmetric spectrum. Thus the spectrum is smoothed without restorting to independent estimates.

◇